The Use of LiDAR in Identifying High-risk Slopes at Sites of Deep-seated Catastrophic Landslides

Naohiro ISOGAI[1,*], Atsuhiko KINOSHITA[1], Teruyoshi TAKAHARA[1], Tadanori ISHIZUKA[1], Osamu YOKOYAMA[2], and Fumi TAKEMURA[2]

[1] Volcano and Debris Flow Research Team, Erosion and Sediment Control Research Group, Public Works Research Institute (Minamihara, Tsukuba-shi, Ibaraki-ken 3058516, Japan)

[2] Japan Conservation Engineers & Co., Ltd. (Toranomon, Minato-ku, Tokyo-To 1050001, Japan)

*Corresponding author. E-mail: n-isogai44@pwri.go.jp

The extraction of mass rock creep slopes is critically important to assess the instability of slopes and predict deep-seated catastrophic landslides. We present a method to extract mass rock creep slopes using airborne laser scanning data (LiDAR). The mass rock creep slopes were extracted quantitatively using the slope gradient ratio and the minimum eigenvalue ratio in different analysis distances, and we expect greater accuracy when both are used in combination.

Key words: mass rock creep, deep-seated catastrophic landslide, eigenvalue ratio, slope gradient

1. INTRODUCTION

When a deep-seated catastrophic landslide (DCL) occurs, large-scale debris flows or landslide dams may cause enormous damage to surrounding areas. It is extremely important to predict the DCL susceptibility for disaster prevention and reduction. Areas particularly prone to DCLs include slopes in which the rock mass has been deformed due to long-term gravity action (hereafter, referred to as mass rock creep slopes) [*Chigira and Kiho*, 1994; *Chigira,* 2009; *Akther et al.,* 2011]. Therefore, extraction of the mass rock creep slopes is useful for predicting areas prone to DCLs. However, fluctuations in mass rock creep slopes are quite small compared to chronic landslides, and their geomorphic characteristics may not be noticeable. Due to vegetation, it is difficult to spot minor geomorphic characteristics of mass rock creep slopes through the conventional interpretation of aerial photographs. In addition, it is difficult to assess wide areas with the same accuracy against the same standards.

Recently, more detailed landform information for the ground surface using the airborne laser (LiDAR) has been obtained [e.g. *McKean and Roering,* 2004; *Glenn et al.,* 2006; *Kasai et al.,* 2009]. Using LiDAR enables one to assess minor geomorphic characteristics, like mass rock creep slopes, quantitatively [*Yokoyama et al.,* 2012]. If geomorphic characteristics can be extracted with a certain accuracy, mistakes in interpretation and oversights can be reduced, and mass rock creep slopes can be extracted with a high degree of accuracy.

In this study, we attempted to extract the mass rock creep slopes quantitatively by using the LiDAR data. We have applied the results of *Yokoyama et al.* [2012] as the extraction method, and in order to validate the adequacy of this method, the extraction results have been compared with those obtained using a conventional method.

2. STUDY AREA AND METHOD

2.1 Study area

The study area was located in the center of the Kii Peninsula (**Fig. 1**). The mountainous Kii Peninsula rises to an elevation of nearly 2000 m, forming steep canyon walls. It belongs to the Cretaceous Shimanto Belt (accretionary complex) in terms of its basement geology, consisting of alternating layers of sandstone and shale, in addition to chert and shale with masses of greenstone. The strata strike northeast–southwest, or east–west, and they dip 30–50° to the north.

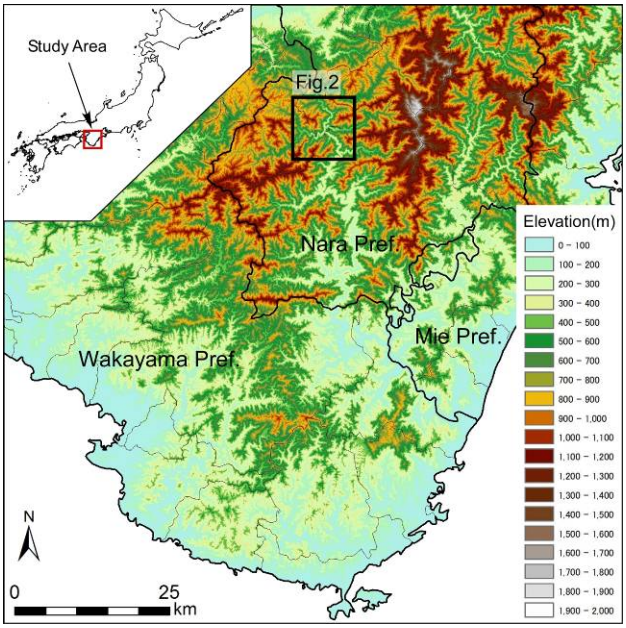

Fig. 1 The study area

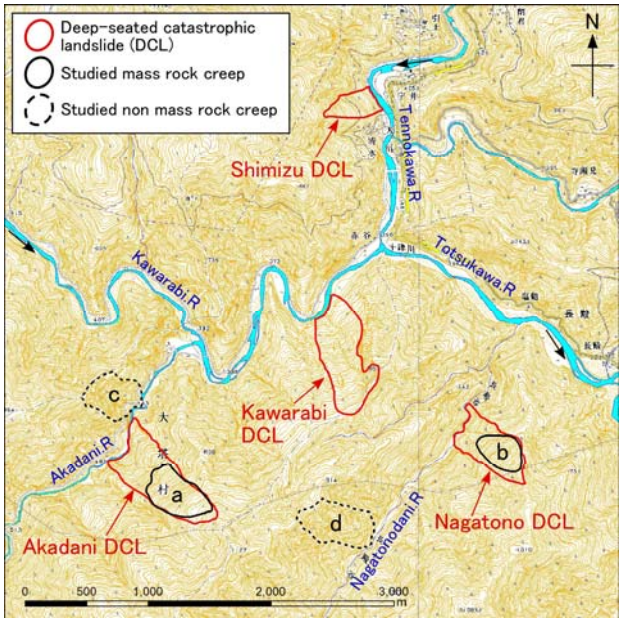

Fig. 2 Extraction area of the mass rock creep slope

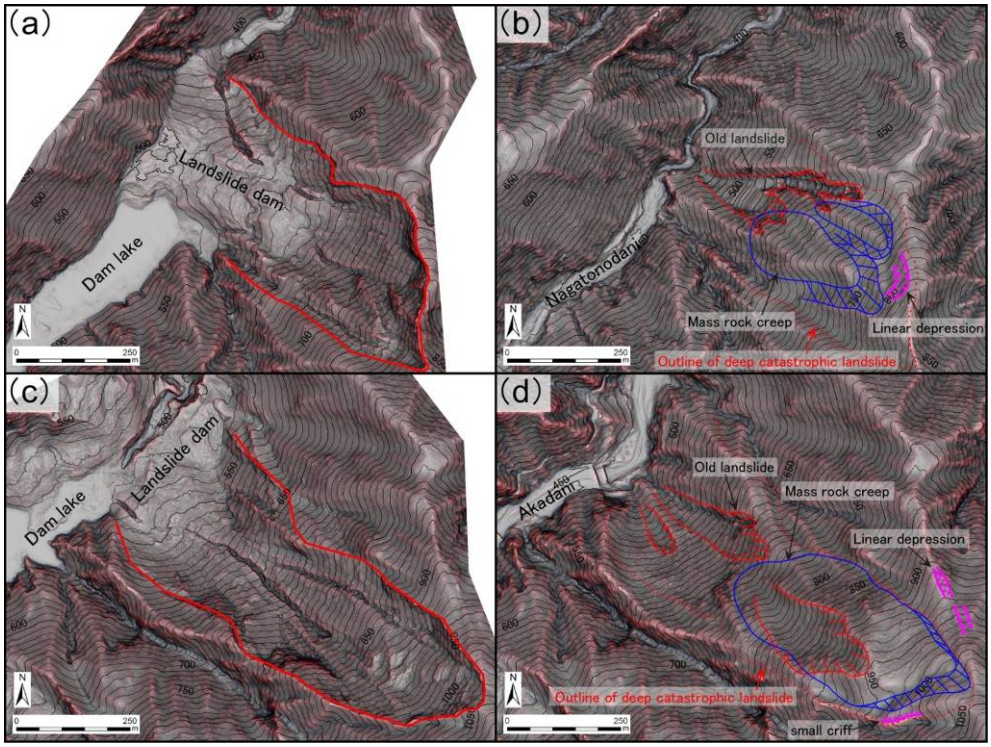

Fig. 3 Landforms before and after the DCLs:

(a) Nagatono after landslide, (b) Nagatono before landslide, (c) Akadani after landslide, (d) Akadani before landslide

Many DCLs occurred in the Kii Peninsula due to Typhoon Talas in September of 2011. Quantitative extraction of the mass rock creep slope using LiDAR was conducted within a ~15 km^2 area in which large-scale DCLs were concentrated (**Fig. 2**).

We determined that these DCLs were mass rock creeps according to aerial photo (taken in 1976, 1/15,000 of the scale size) interpretation, map reading, and field surveys. However, in the slopes that DCL did not occur, many mass rock creeps was included. In this study, we targeted the studied mass rock creep slope (a) and (b) in **Fig.2**. The studied non-mass rock creep slope (c) and (d) were also selected by the same method in many non-mass rock creep slopes. Especially the non-mass rock creep slope is steep and high valley density compared with the mass rock creep slope.

The landforms of the representative slopes

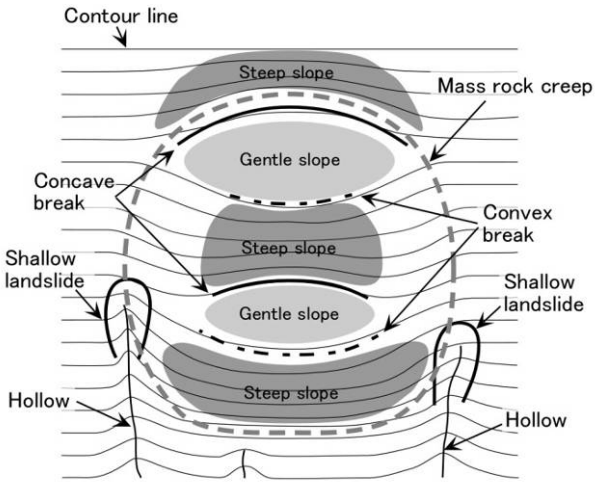

Fig. 4 Geomorphic characteristics of mass rock creep slopes (According to *Yokoyama et al.,* [2012])

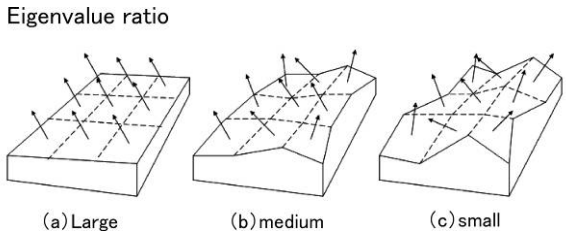

Fig. 5 Conceptual diagram of eigenvalue ratio (According to *Uchida et al.,* [2010])

before and after the DCLs are shown in **Fig. 3**. Before the DCL in Akadani, the upper part exhibited a moderate slope and the lower part a steep slope; these geomorphic characteristics are the same as those of the general mass rock creep slopes (**Fig. 4**). The slope was low relief, with no deep valley, compared to the surrounding areas; while the same was true in Nagatono. The mass rock creeps of Akadani and Nagatono will be referred to as "Slope (a)" and "Slope (b)" in this paper.

The non-mass rock creep slopes were extracted around the mass rock creep slopes. They were the slopes on the deep valley sides without convex and concave breaks in the slopes; the areas were approximately equal to the mass rock creep.

2.2 Quantitative extraction method of mass rock creep slopes

2.2.1 Geomorphic characteristics of mass rock creep slope

In general, mass rock creep slope geomorphic characteristics include the following: (1) no deep valley or stream in the moving zone, (2) paired concave and convex breaks of slope in the moving zone, (3) small valleys or small landslides formed at the boundaries on both sides of the moving zone, and (4) a steep escarpment located around the upper boundaries of the moving zone, facing the valley (**Fig. 4**). *Yokoyama et al.* [2012] showed that the first two geomorphic characteristics in this list could be represented by quantitative indexes using LiDAR data. They calculated the slope gradient and eigenvalue ratio for both mass rock creep slopes and non-mass rock creep slopes.

2.2.2 Geomorphological condition

The slope gradient was calculated based on the method of Burrough and McDonell. When the center cell elevation (coordinate values of x, y) in a 3 × 3 grid cell is $Z_{x,y}$, the slope gradient I (rad) can be calculated using formula (1):

$$I = \operatorname{atan}\sqrt{(dz/dx)^2 + (dz/dy)^2} \tag{1}$$

$$\frac{dz}{dx} = \frac{1}{8D}\{(Z_{x-1,y+1} + 2Z_{x-1,y} + Z_{x-1,y-1}) - (Z_{x+1,y+1} + 2Z_{x+1,y} + Z_{x+1,y-1})\} \tag{2}$$

$$\frac{dz}{dy} = \frac{1}{8D}\{(Z_{x-1,y+1} + 2Z_{x,y+1} + Z_{x+1,y+1}) - (Z_{x-1,y-1} + 2Z_{x,y-1} + Z_{x+1,y-1})\} \tag{3}$$

where I is the slope gradient, dz/dx is the rate of elevation change from the center cell in the x direction and dz/dy is the rate of elevation change from the center cell in the y direction, expressed in the formulas (2) and (3), respectively. D is the analysis distance (analysis size).

The eigenvalue ratio recognizes disturbances of the normal vector to the slope as ground surface disturbances, indicating the degree of unevenness (**Fig. 5**). A large eigenvalue ratio indicates a low relief and smooth surface, and a small eigenvalue ratio indicates large surface roughness. The eigenvalue ratio was calculated based on the method of Woodcock and Naylor. When the azimuth angle is φi and the zenith angle is θi in the 3 × 3 grid cell i, the normal vector (x_i, y_i, z_i) of the grid cell i can be expressed by formula (4):

$$(x_i, y_i, z_i) = (\cos\theta_i \cos\varphi_i, \cos\theta_i \sin\varphi_i, \sin\theta_i) \tag{4}$$

The tensor T, the direction of the normal vector, is expressed in formula (5):

$$T = \begin{bmatrix} \sum x_i^2 & \sum x_i y_i & \sum x_i z_i \\ \sum y_i x_i & \sum y_i^2 & \sum y_i z_i \\ \sum z_i x_i & \sum z_i y_i & \sum z_i^2 \end{bmatrix} \tag{5}$$

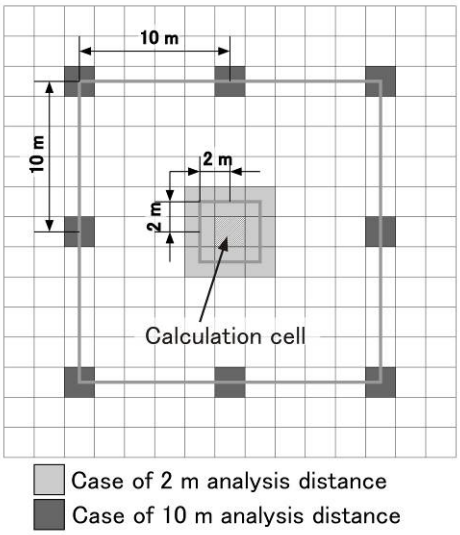

Fig. 6 Conceptual diagram of the analysis distance (According to *Yokoyama et al.,* [2012])

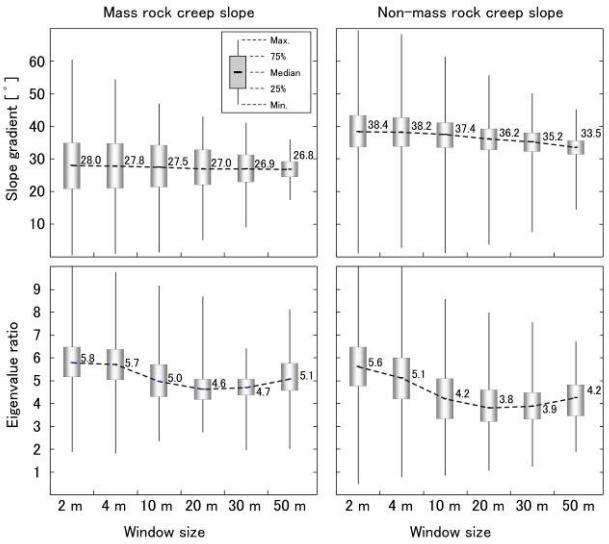

Fig. 7 Box plot diagrams showing changes in slope gradient and eigenvalue ratio (According to *Yokoyama et al.,* [2012])

The eigenvalues (λ_1, λ_2, λ_3, in descending order) of this matrix T are calculated, and then S_1 and S_2 are calculated using formula (6):

$$S_i = \frac{\lambda_i}{\lambda_1 + \lambda_2 + \lambda_3} \quad (6)$$

By using S_1 and S_2, the eigenvalue ratio γ is calculated using formula (7):

$$\gamma = \ln(S_1 / S_2) \quad (7)$$

To calculate the geomorphological condition, *Yokoyama et al*. [2012] gradually increased the intervals between eight cells used for calculation, referred to as the analysis distance (**Fig. 6**). For example, in the case of a 10 m analysis distance, we used elevation data that located the 10 m interval from the calculation cell. Changing the analysis distance enables the expression of landform information at large spatial scales while keeping the digital elevation model (DEM) point density high.

Box plot diagrams of the slope gradient and eigenvalue ratio in both the mass rock creep slope and non-mass rock creep slope are shown in **Fig. 7**. For the mass rock creep slope, the median of the slope gradient is constant, regardless of the analysis distance (upper left in **Fig. 7**). For the non-mass rock creep slope, the median of the slope gradient gradually becomes smaller with greater analysis distance (upper right in **Fig. 7**). The median of the eigenvalue ratio for the mass rock creep slope is lowest for a 20 m analysis distance (lower left in **Fig. 7**). For the non-mass rock creep slope, the median of the eigenvalue ratio is also lowest for a 20 m analysis distance and is lower than the mass rock creep slope (lower right in **Fig. 7**). Based on this, we expected that the mass and non-mass rock creep slopes could be separated by calculating the slope gradient and the eigenvalue ratio using different analysis distances.

2.2.3 Method to extract mass rock creep slopes

A flow diagram for the method used to extract the mass rock creep slopes is shown in **Fig. 8**. The adopted LiDAR data were obtained before the DCLs occurred in the study area. First, the 2 m grid DEM was created based on the LiDAR data. Next, the slope gradient and eigenvalue ratio were calculated using 15 different values of the analysis distance from 2-500 m. Box plot diagrams of the slope gradient and eigenvalue ratio for the representative mass rock creep slopes and non-mass rock creep slopes in the study area are shown in **Fig. 9**. The slope gradient greatly decreased when the analysis distance was larger than 100–200 m, which can be attributed to the analysis distance substantially exceeding the landform scale of the mass rock creep slope. To separate the two slope types, a certain analysis distance is required. In addition, the eigenvalue ratio pattern for an analysis distance >100 m in the median differs from the distinctive pattern of mass rock creep slopes. Accordingly, we decided to use an analysis distance up to 100 m in this study. Next, we performed median processing on 50 meters squared, the median in the box plot diagrams, to extract a mass rock creep slope of about 100 m in width (minimum). Finally, we calculated the slope gradient ratio and the eigenvalue ratio.

Since the absolute quantity of the slope gradient

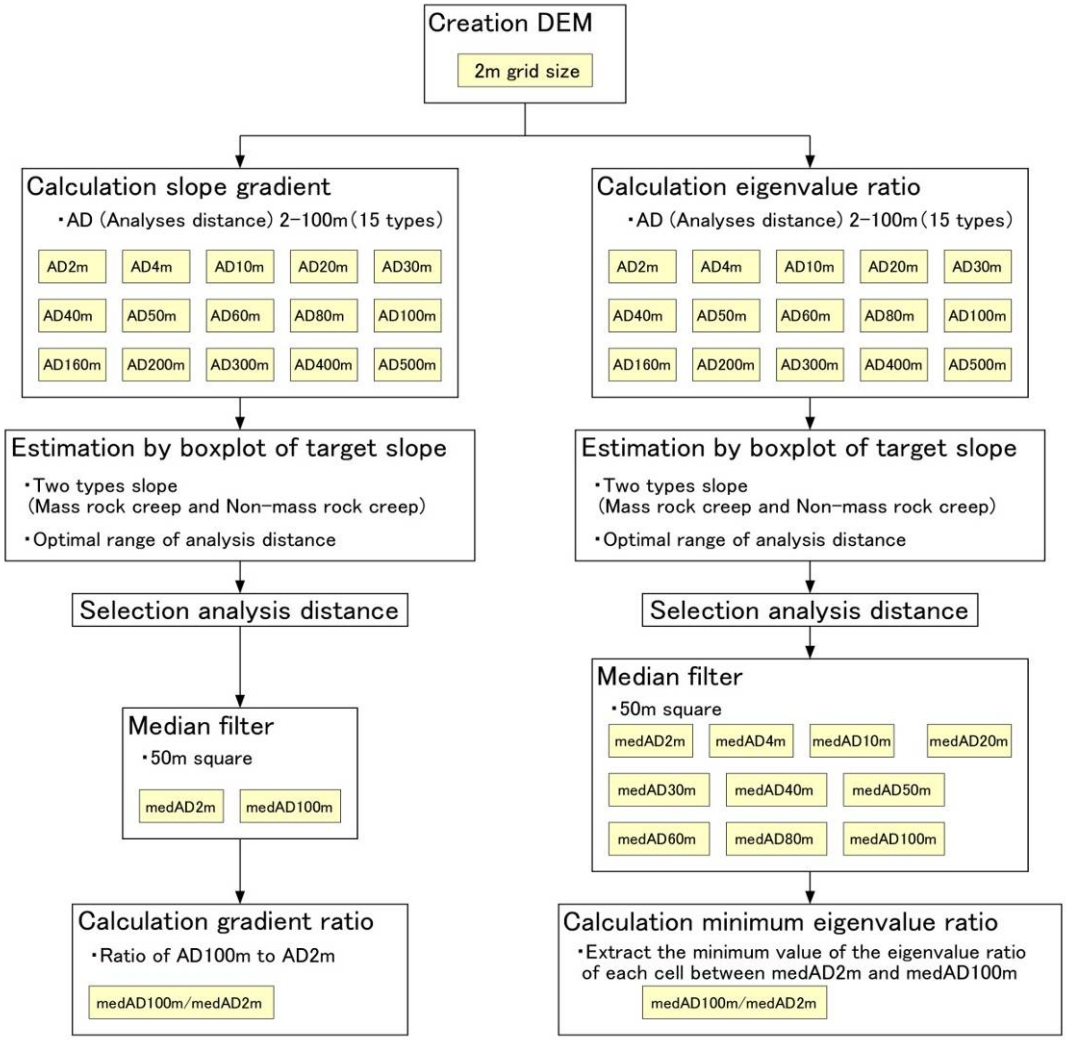

Fig. 8 Flow to extract mass rock creep

for both slope types differs substantially, we adopted the ratio of the minimum and maximum analysis distance to assess change. For example, the slope gradient ratio of the mass rock creep slope was ~1.0, while that of the non-mass creep slope was ~0.7. The eigenvalue ratio of the minimum analysis distance for each cell was selected for analysis distances in the range 2-100 m. For example, the minimum eigenvalue ratio for the mass rock creep slope was 4.3, while the non-mass rock creep slope was 2.8

3. RESULTS

The distributions of the slope gradient ratio and the minimum eigenvalue ratio are shown in **Fig. 10**. In the slope gradient ratio distribution, the blue and red bands and the areas in the yellow to pale red color are mixed (upper panels in **Fig. 10**). Wide rivers appear as dark red bands, with slope gradient ratios of at least 1.2. Meanwhile, valleys and ridges appear as blue bands, with slope gradient ratios of 0.7 or below. Regions in yellow to pale red have slope gradient ratios that lie between these two values. The distribution of the eigenvalue ratios was similar to the slope gradient ratios (lower panels in Fig. 10). Valleys and ridges appear as yellow to red bands. In other words, the minimum eigenvalue ratios are shown as values of 2 or lower. In contrast to the slope gradient ratio, only the river is emphasized as a large value.

The slope gradient ratio was substantially different between the mass rock creep slope and the non-mass rock creep slope. In Slope (a), the area with the slope gradient ratio of ~1 was large part. The same applies to Slope (b), where the non-mass rock creep slope area with slope gradient ratio of 0.85 or lower was large.

The minimum eigenvalue ratio was also

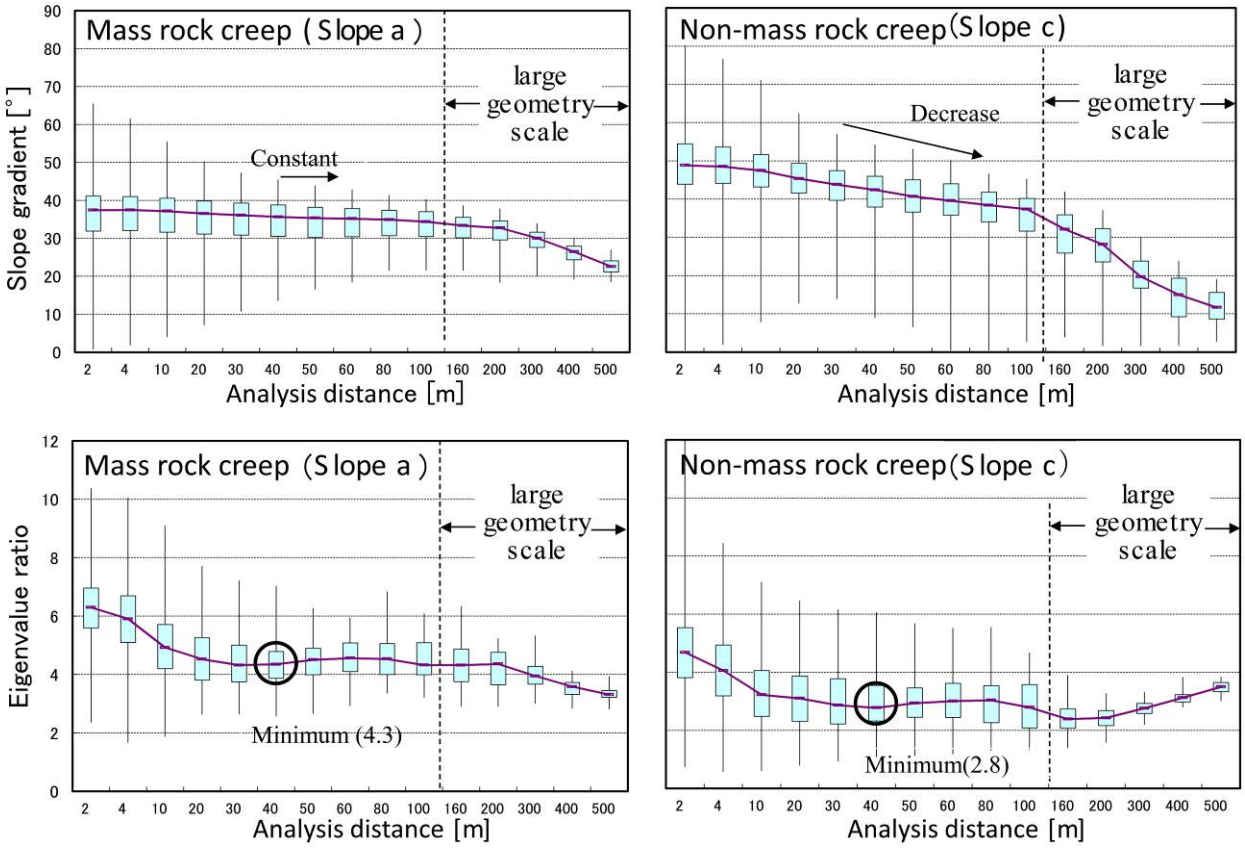

Fig. 9 Box plot diagrams of the mass rock creep slope and non-mass rock creep slope in the studied area

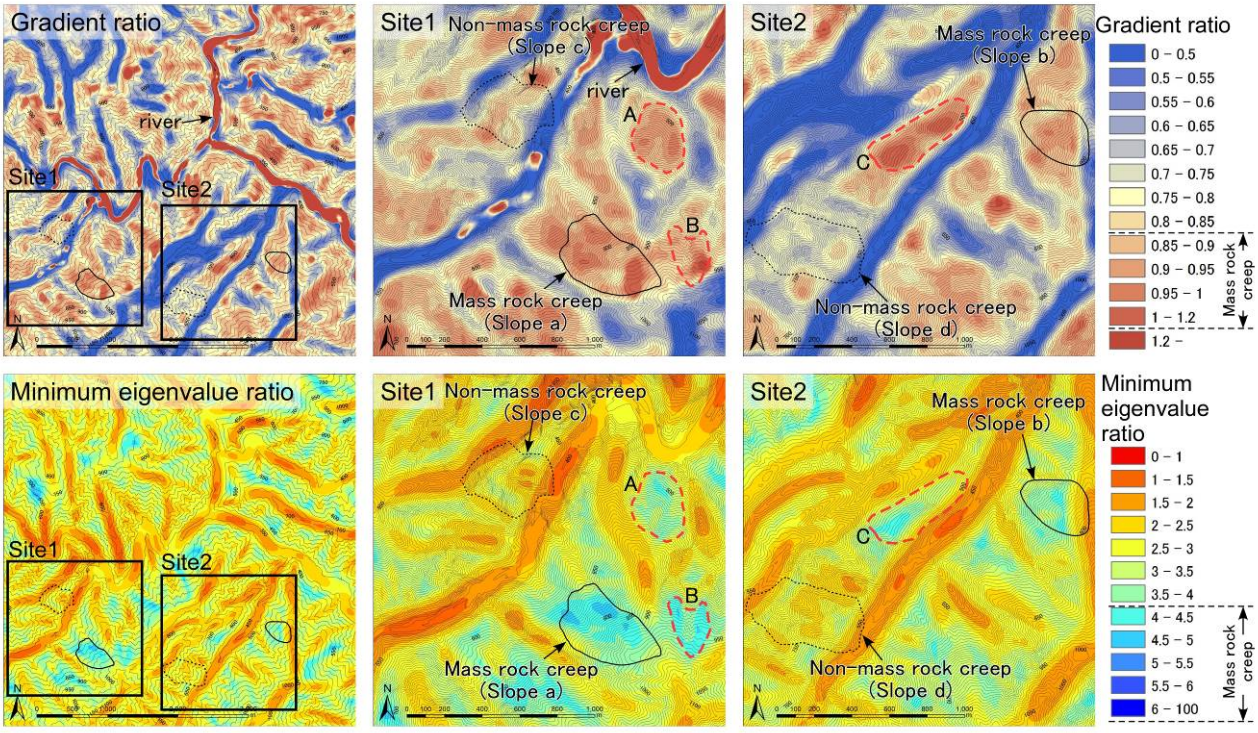

Fig. 10 Result of extraction of mass rock creep slopes:
top: extraction result based on slope gradient ratio, bottom: extraction result based on minimum eigenvalue ratio

substantially different in the mass rock creep slope and the non-mass rock creep slope. In the mass rock creep slopes in both Slope (a) and Slope (b), the minimum eigenvalue ratio was 4 or higher;

conversely, it was 3 or lower in the non-mass rock creep slopes.

4. DISCUSSION

The slope gradient ratio and the minimum eigenvalue ratio of the mass rock creep slopes differed from other types of slopes, providing a way to distinguish them. A slope gradient ratio of 0.85 or higher indicates a mass rock creep slope. However, the slope gradient ratio in flats, including riverbeds, was 1.2 or higher; thus, it is beneficial to exclude riverbed areas. A minimum eigenvalue ratio of 4 or higher generally indicates a mass rock creep slope. These values are consistent with the predicted thresholds in the box plot diagrams (e.g., Slope (a), **Fig. 9**).

Some slopes in the surrounding area have similar values to Slope (a) and Slope (b) (i.e., slopes A, B, and C in **Fig. 10**). Slope A represents Kawarabi, where the DCL shown in **Fig. 2** occurred, validating this mass rock creep extraction method.

Using the slope gradient ratio showed a wider mass rock creep area than that in the extraction result using the minimum eigenvalue ratio, because using the slope gradient ratio may also include less well-developed mass rock creep slopes. In other words, extraction using the eigenvalue ratio only covers well-developed mass rock creep slopes, narrowing the result.

By changing the geomorphological condition index threshold, it is possible to refine detection of the mass rock creep slopes. Further, it may be possible to refine the results by overlapping two types of diagrams. The setting thresholds and extraction result should be verified in the future. In addition, the risk of DCLs in the extracted mass rock creep slopes should be assessed.

5. CONCLUSION

We presented a method to extract mass rock creep slopes using LiDAR data. The study made the following points clear.

1. The slope gradient ratio and the minimum eigenvalue ratio calculated under different analysis distances were useful indexes that quantitatively distinguished between mass rock creep slopes and non-mass rock creep slopes.
2. It was possible to refine mass rock creep slope detection by setting thresholds and overlapping.
3. Using these ratios in combination, mass rock creep slopes can be extracted with greater accuracy.

ACKNOWLEDGEMENT: The authors express our gratitude and wish to acknowledge helpful advice and comments offered by the members of the Erosion and Sediment Control Research Group of the Public Works Research Institute, and officials in the Erosion and Sediment Control Division, Research Center for Disaster Management, National Institute for Land and Infrastructure Management, Ministry of Land, Infrastructure, Transport and Tourism. In particular, we thank Ms. Ai Kawakami, former part-time personnel, who assisted in the GIS work.

REFERENCES

Akther, H., Shimokawa, E., Teramoto, Y. and Jitousono, T. (2011) : Geomorphological features and prediction of potential sites for deep□seated landslides on Wanitsuka Mountain, Miyazaki Prefecture, Japan, Journal of Japan Society of Erosion Control Engineering, Vol. 63, No. 5, p. 14–21

Chigira, M. and Kiho, K. (1994) : Deep-seated rockslide-avalanches preceded by mass rock creep of sedimentary rocks in the Akaishi Mountains, central Japan, Engineering Geology, Vo. 38, p. 221–230

Chigira, M. (2009) : September 2005 rain-induced catastrophic rockslides on slopes affected by deep-seated gravitational deformations, Kyushu, southern Japan, Engineering Geology, Vol. 108, p. 1–15

Glenn, N. F., Streutker, D. R., Chadwick, D. J., Thackray, G. D. and Dorsch, S. J. (2006) : Analysis of LiDAR-derived topographic information for characterizing and differentiating landslide morphology and activity, Geomorphology, Vol. 73, p. 131–148

Kasai, M., Ikeda, M., Asahina, T. and Fujisawa, K. (2009) : LiDAR-derived DEM evaluation of deep-seated landslides in a steep and rocky region of Japan. Geomorphology, 113, p. 57–69

McKean, J. and Roering, J. J. (2004) : Landslide detection and surface morphology mapping with airborne laser altimetry, Geomorphology, Vol. 57, p. 331–351

Uchida, T., Nakano, Y., Akiyama, K. Tamura, K., Kasai, M., Suzuki, R. (2010) : The role of LiDAR data on evaluation of shallow landslide susceptibility and detection of mass-rock creeping slope, Transactions, Japanese Geomorphological Union, Vol. 31, No.4, p. 383–402

Yokoyama, O., Uchida, T., Nakano, Y., Ishizuka, T., Kasai, M. and Suzuki, R. (2012) : Clarifying surface shape of mass rock creep revealed by using airborne LiDAR, Japan, Journal of Japan Society of Erosion Control Engineering, Vol. 64, No. 6, p. 13–24